Friedrich Wahl Samuel So Kwan Wong

A Hybrid Optical-Digital Image Processing Method for Surface Inspection

A hybrid measurement technique is proposed for high-precision surface inspection. The technique uses an interferometer to image microscopic surface defects. In order to quantify the degree of various surface defects, the interferograms are scanned, digitized, and subsequently converted to a binary image by using an adaptive thresholding technique which takes into account the inhomogeneity of the imaging system. A new misalignment measure for binary patterns identifies the "straightness" of the fringe lines. It is shown that the resulting percentages of misaligned picture elements conform fairly well with the degree of various surface defects.

Introduction

High-precision surface quality inspection is very important in many industrial applications, e.g., in magnetic disk and in semiconductor wafer manufacturing. This paper describes a hybrid optical-digital image processing method to detect microscopic surface defects, such as voids, cracks, scratches, and asperities, having dimensions in the range of a few micro-inches. Although we have applied our proposed

Reference image

Reference objective lens

Sample objective lens

Sample objective lens

Figure 1 Principle of the Linnik Interference Microscope.

inspection method to magnetic disks, the principle can be applied to many surface quality inspection problems.

Interferometry is a well-known noncontact optical technique which can provide three-dimensional microscopic measurements of a surface [1-3]. Surface deviations normal to the surface plane are indicated by the deviations of fringe lines. An interferometer is a useful tool for qualitative examination of surface finishes. Quantitative measurements can also be made by manually measuring all deviations relative to the fringe separation. However, this is a very time-consuming process, particularly for microscopic measurements over such large areas as disk surfaces.

In this paper a fast and reliable technique is described for quantifying interferometric measurements on any given surface. The interference fringe patterns are scanned by a high-resolution TV camera and digitized. The digitized images are then analyzed, taking into account the nonuniform shading effects caused by the imaging process. Subsequently, a spacially adaptive thresholding operation is applied, producing binary fringe lines. The fringe deviations caused by surface defects are then measured as the degree of misalignment in the binary fringe lines. This algorithm produces a single number—a misalignment percentage—

© Copyright 1983 by International Business Machines Corporation. Copying in printed form for private use is permitted without payment of royalty provided that (1) each reproduction is done without alteration and (2) the *Journal* reference and IBM copyright notice are included on the first page. The title and abstract, but no other portions, of this paper may be copied or distributed royalty free without further permission by computer-based and other information-service systems. Permission to *republish* any other portion of this paper must be obtained from the Editor.

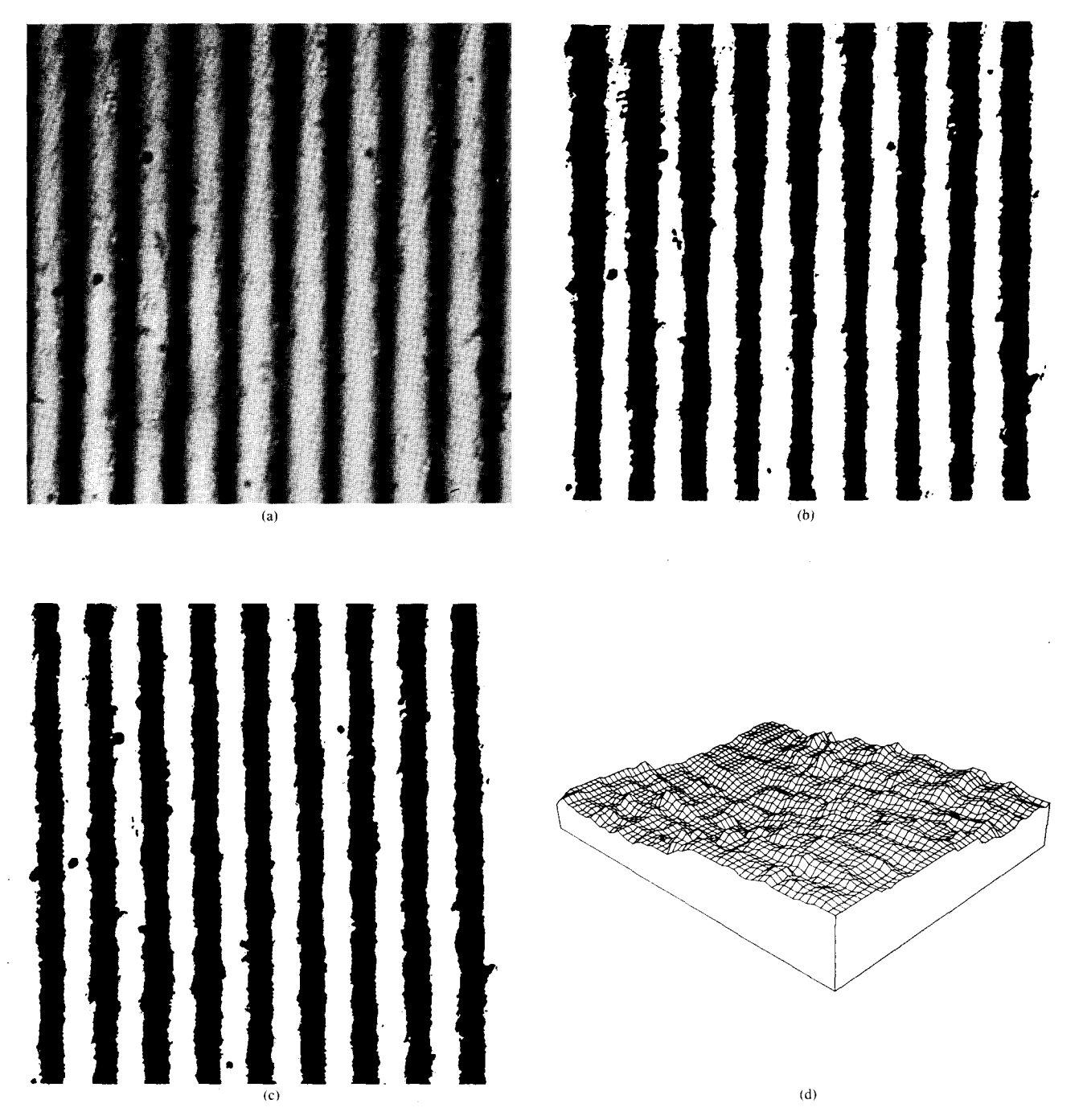


Figure 2 Interferogram (1): (a) Interferogram of a flat polished surface. (b) Space-invariant and (c) space-variant thresholded interferograms. (d) Reference image for space-variant thresholding of interferogram (minimum gray level: 147; maximum gray level: 177).

for each interferogram. The results of this paper show that misalignment percentage increases directly as more serious defects appear on the surface. Therefore, the proposed technique should be a powerful tool in manufacturing inspection to determine whether a surface has serious defects. However, the misalignment measure proposed here does not

determine defect types, e.g., voids, cracks, asperities. Further analysis is required for defect type classification.

Principle of interferometric measurement

The interferometer used in this experiment is a Leitz Linnik Interference Microscope [4]. It is a modified arrangement of

377

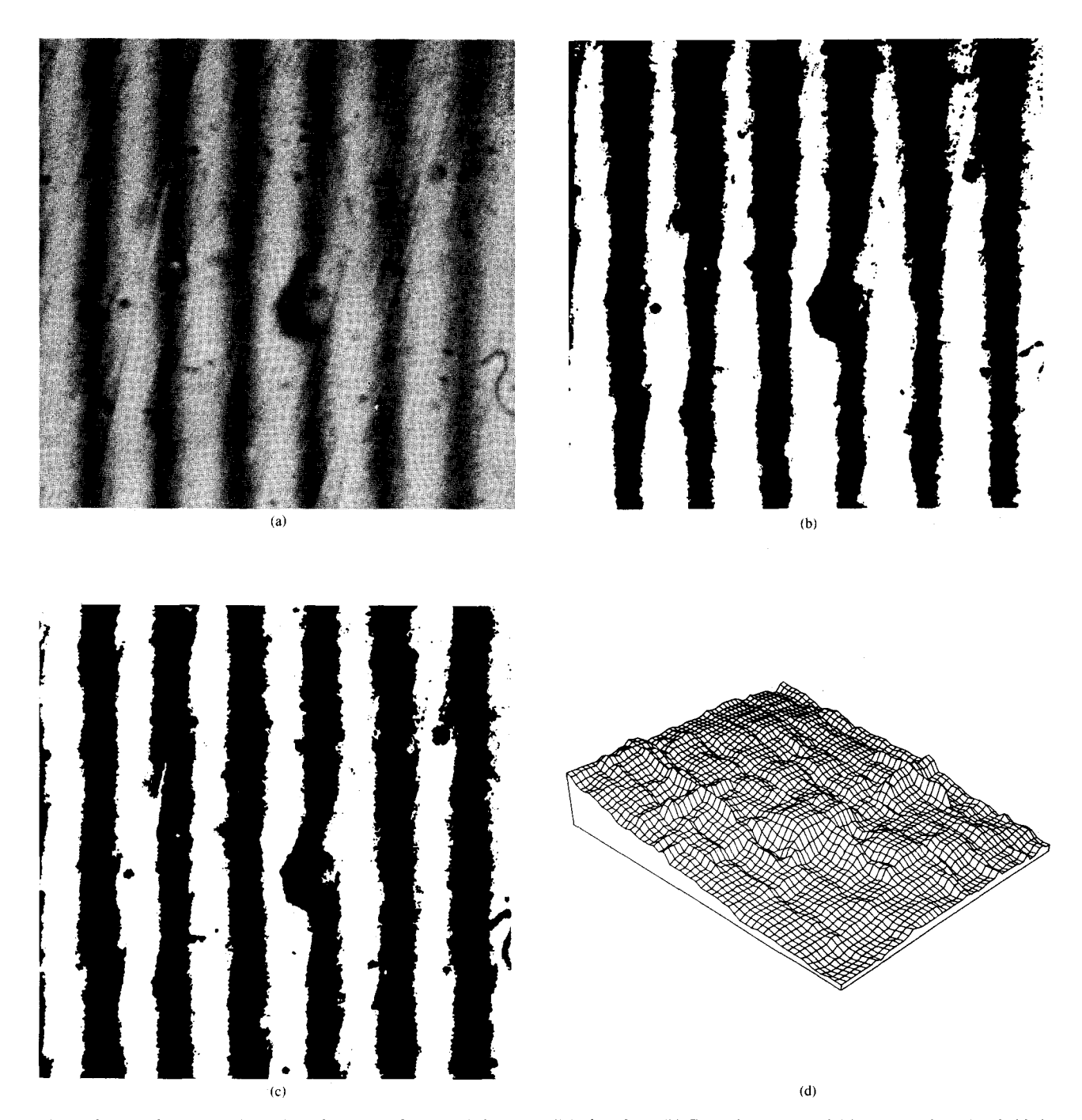


Figure 3 Interferogram (2): (a) Interferogram of a small hole on a polished surface. (b) Space-invariant and (c) space-variant thresholded interferograms. (d) Reference image for space-variant thresholding of interferogram (minimum gray level: 134; maximum gray level: 174).

the well-known Michelson interferometer with a matched pair of objective lenses placed in the sample and reference light beam paths, as shown in Fig. 1. The incident light beam is split by a beam splitter into two coherent beams with equal intensity. After reflection from equidistant reference and sample surfaces, the two light beams are recombined by the beam splitter. If the reference mirror is adjusted to have a

small wedge angle, α , the interference fringes can be observed in the image plane. The fringe separation can be increased by decreasing the wedge angle. When the wedge angle $\alpha=0$, the reference mirror becomes a plane-parallel plate. In this case the fringe width becomes infinite. The alternate bright and dark fringes are produced by the constructive and destructive waves from the sample and

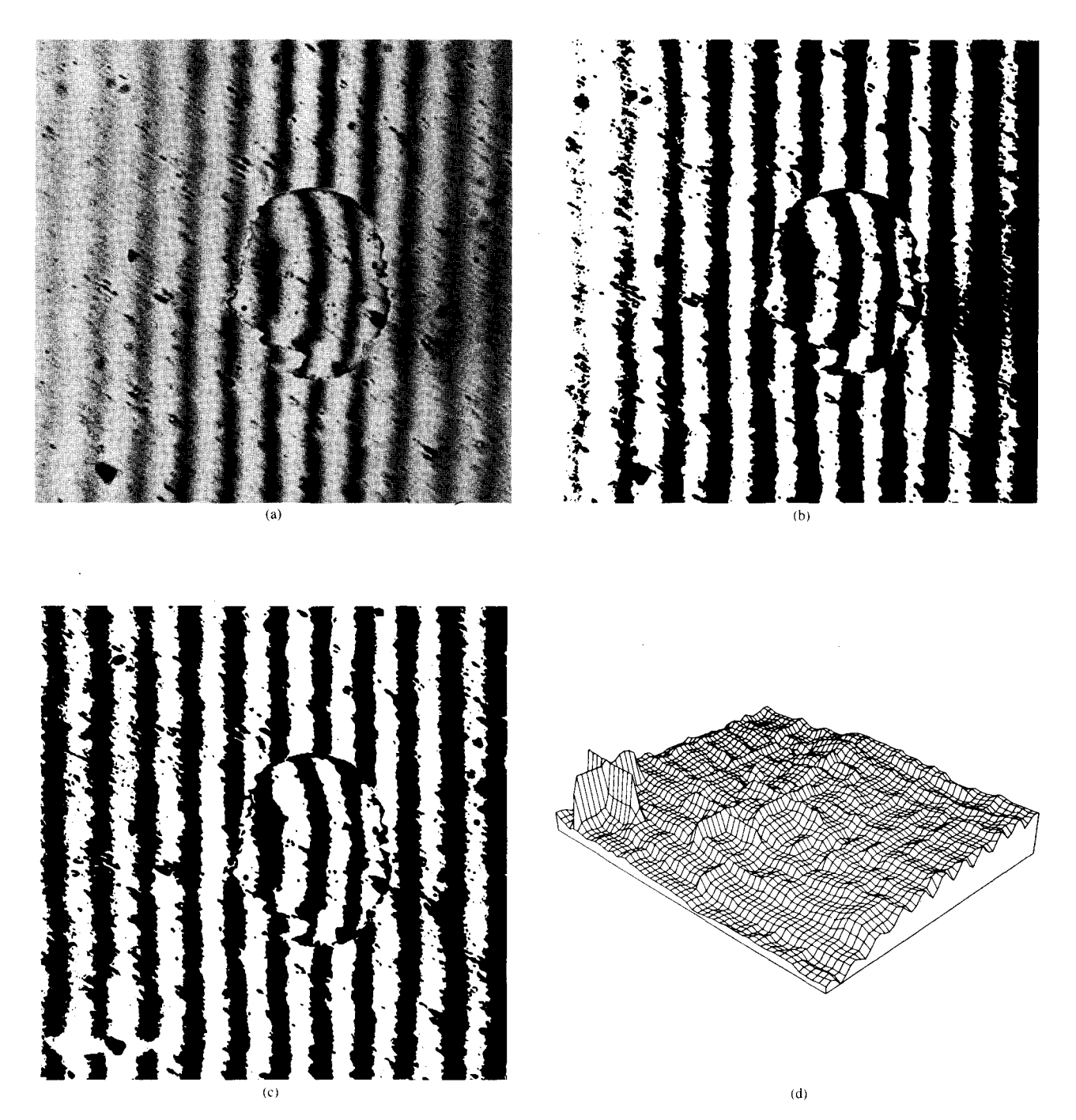


Figure 4 Interferogram (3): (a) Interferogram of a liquid stain on a polished surface. (b) Space-invariant and (c) space-variant thresholded interferograms. (d) Reference image for space-variant thresholding of interferogram (minimum gray level: 96; maximum gray level: 147).

reference beams. The constructive interference occurs when the path difference is an odd multiple of a quarter wave length. The destructive interference occurs at even multiples of a quarter wave length. The fringe-to-fringe spacing is therefore simply equal to half of the wave length. The fringe spacing always corresponds to a vertical height of $\lambda/2$ normal to the surface plane. Thus, the ratio of the fringe deviation

from the parallel interference fringes to the fringe period determines the variation of the height of a local surface area.

Interferograms of typical surface defects

The sample used in the interferometric measurements to be described is a coupon of polished aluminum substrate with

379

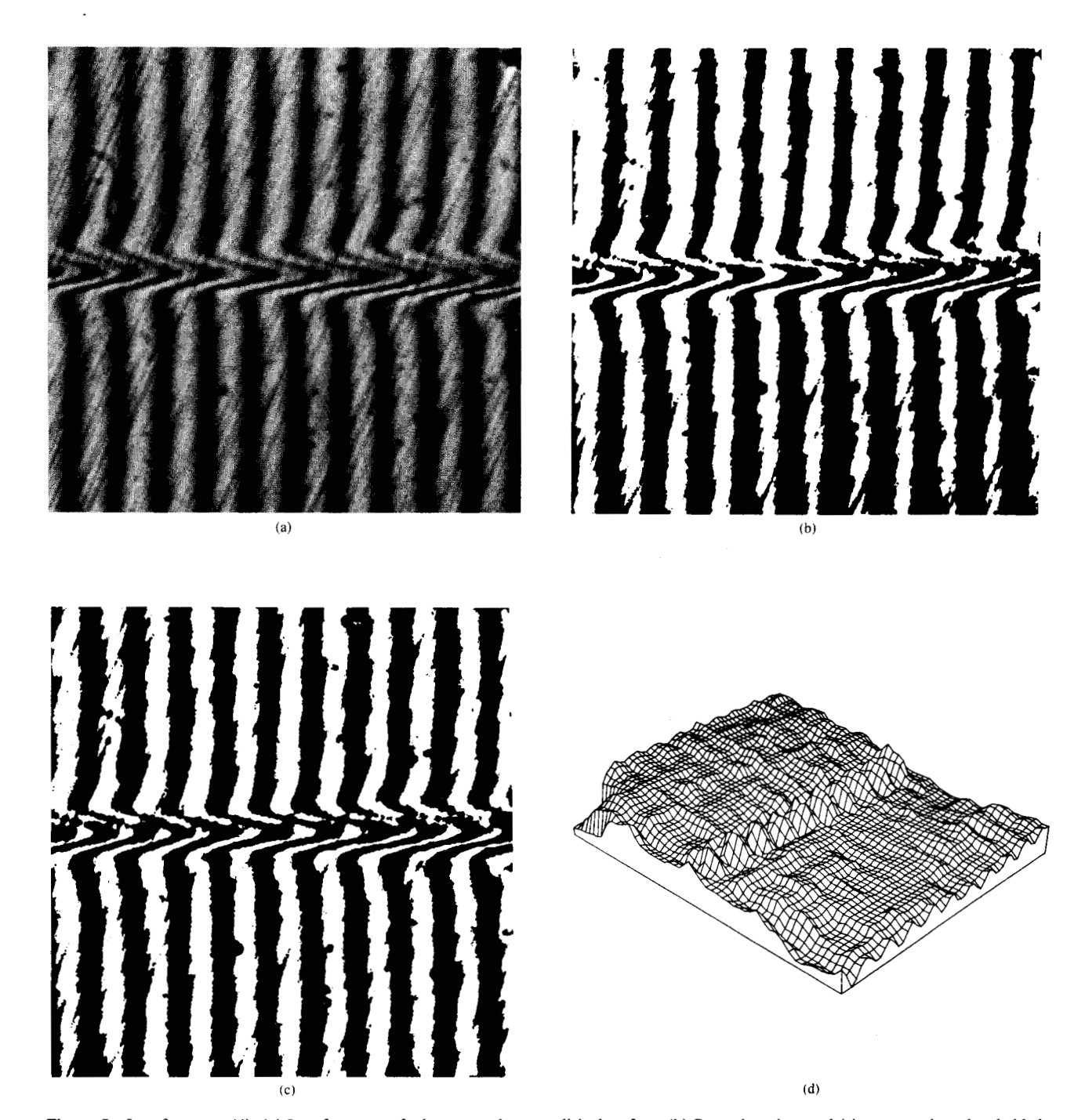


Figure 5 Interferogram (4): (a) Interferogram of a long scratch on a polished surface. (b) Space-invariant and (c) space-variant thresholded interferograms. (d) Reference image for space-variant thresholding of interferogram (minimum gray level: 109; maximum gray level: 155).

many surface irregularities. Figures 2(a)-6(a) show some interference fringe patterns on this surface using $10 \times$ matched-pair objective lenses with 100:1 magnification. A green filter ($\lambda = 546$ nm) is used to generate these fringes, so that the fringe-to-fringe distance corresponds to 273 nm. The parallel straight fringes in Fig. 2(a) indicate a flat surface. The fuzziness on both sides of each fringe is caused by surface roughness. The polishing mark can be seen in the

background oriented at an angle to the fringe lines. Figure 3(a) shows the interference pattern of an elongated small hole on the surface, while Fig. 4(a) shows the interference pattern for a liquid stain on a polished metal surface. The nonuniform fringe contrast is caused by the use of white light in this example, rather than the monochromatic light used in the other examples. Note that the three fringes within the stain have shifted differently, indicating that the liquid stain

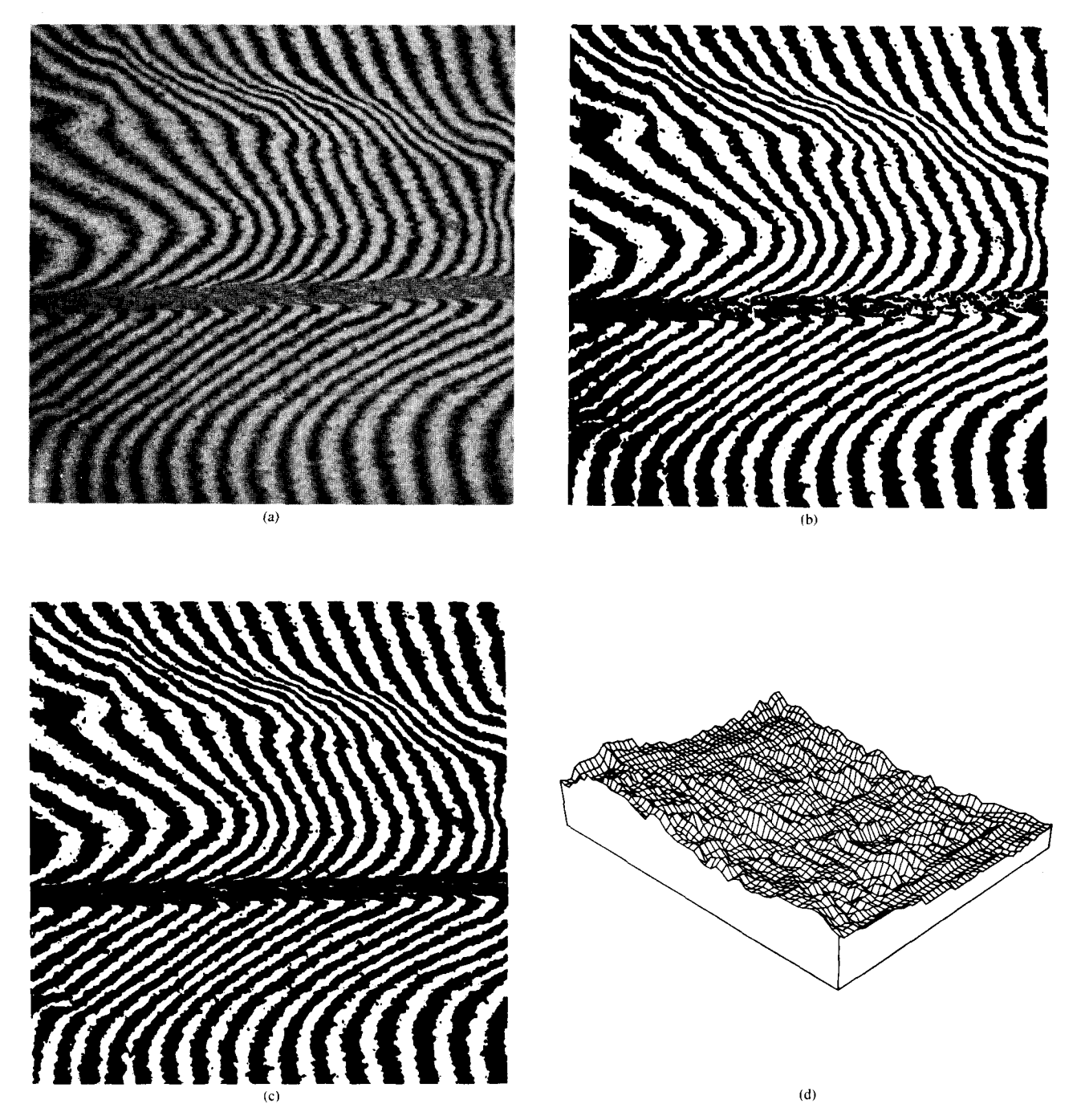


Figure 6 Interferogram (5): (a) Interferogram of a large depression on a polished surface. (b) Space-invariant and (c) space-variant thresholded interferograms. (d) Reference image for space-variant thresholding of interferogram (minimum gray level: 111; maximum gray level: 139).

has nonuniform thickness. Figure 5(a) shows the interference pattern of a long scratch about 50 μ m wide and 500 nm deep. Figure 6(a) shows the interference pattern of a large depression varying in depth from about 0.8 μ m in the bottom to about 2–3 μ m at the top. These examples illustrate the advantage of interferometry over the regular microscope in surface irregularity measurements. The examples shown were then digitized [512 \times 512 8-bit picture elements

(pixels)] for further digital image analysis as described in the following text.

Shading correction of the digitized interferograms

Because the illumination within the object plane, as well as the sensitivity of the sensor in an optical setup such as described earlier, usually has spacial variations, a necessary

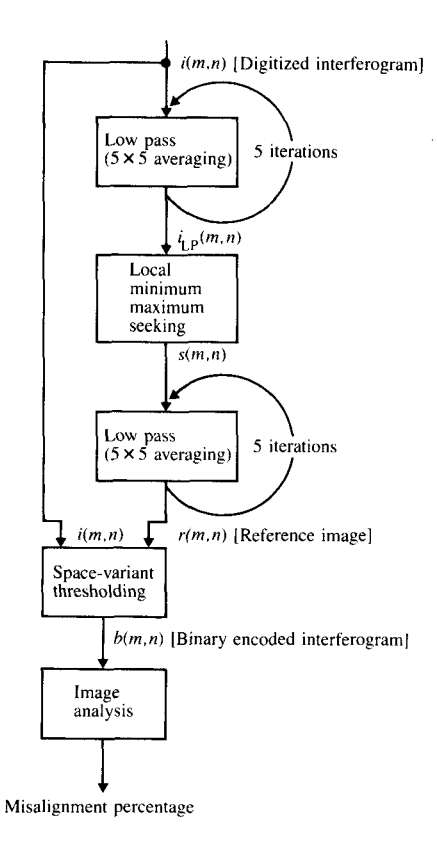


Figure 7 Block diagram of the digital interference pattern analysis.

first processing step prior to thresholding is the compensation of such inhomogeneities. Such a shading correction can be done, e.g., in either of the following two ways:

- Analysis of the variations in illumination and sensor characteristics and subsequent gray level rescaling of the images to be processed. In this case, the subsequent binary encoding can be achieved by means of a simple constant thresholding operation.
- Calculation of a reference image by analyzing the illumination and sensor inhomogeneities. The reference image is used as a spacially varying threshold in this case.

We used approach (2). Because the illumination and the sensor characteristics can be considered as constant system parameters, the reference image has to be calculated only once. Approach (2) has the advantage that the shading correction and the binary encoding are reduced to an element-by-element comparison of the digitized fringe patterns with a threshold reference image. Adaptive thresholding is a well-known concept in image processing [5]. Here we propose a new adaptive thresholding method to estimate the local mean value of a large window area.

The threshold image can be derived easily from any fringe pattern. It is well known that light intensities recorded from parallel fringe lines can be described by a cos² function along an axis perpendicular to the fringe lines. Due to the physical realization of the interferometric measurement setup, this function is distorted additively as well as multiplicatively in a space-variant manner, as can be seen from Figs. 2(a)-6(a). An ideal thresholding value would be the local mean value of this function. This mean value could be calculated by means of an averaging operation within a local window large enough to cover multiples of the cos² function period. In the case of curved fringe lines, an appropriate window size is difficult to define and depends on the pattern to be processed itself. In order to have reasonable accuracy in determining the surface deviations, each period of the fringe line must be scanned with a fairly large number of pixels; in our experiment a period of the fringe line correponds to about 50 pixels. To calculate the local mean value of the cos² function, one has to use a window size of (50×50) , which takes a lot of computation time. In order to avoid such large-size window averaging, we use a minimum and maximum gray level seeking operation within a local cross which covers at least one period of the fringe patterns. The local cross used has 64 pixels horizontally and 64 pixels vertically. Sub-sampling is used to reduce the amount of computation; i.e., one out of three samples is used along the cross to determine the maximum and the minimum. The average value of the local minimum and maximum is used as the local threshold value.

Because the minimum-maximum operation is sensitive to noise, a low-pass filter operation has been applied both prior to and subsequent to the minimum-maximum seeking (see Fig. 7). In the experiments described in this paper, we used a 5 by 5 constant weight averaging operation, which has been applied iteratively five times to the gray level image data. The transfer function of this low-pass filter is rather uncritical if it is assumed that the spacial frequency content of the fringe patterns and the shading function are far enough separated from each other in the spacial frequency domain. This assumption is reasonable in our case. The spacial cutoff frequency of the low-pass filter has to be determined in order to retain the low-frequency shading signal and to suppress the fringe patterns as well as possible.

The necessity of a shading correction can easily be demonstrated by comparing the binary images obtained by means of a constant threshold operation [Figs. 2(b)-6(b)] with those obtained by the method described above [Figs. 2(c)-6(c)]. Clearly, the fringe lines have a more uniform appearance in the latter case. In our experiments the spacially varying threshold function has been calculated for each image separately, because different calibrations of the interferometer have been used for each measurement. These

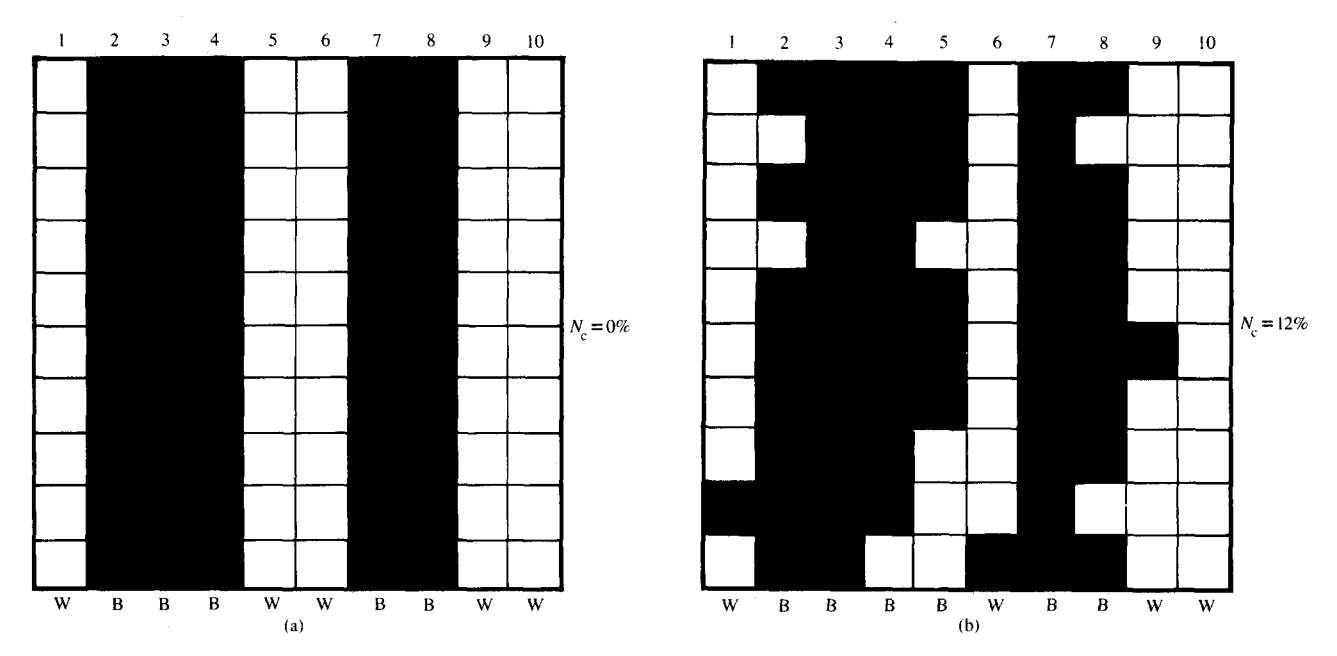


Figure 8 Principle of the misalignment measure. (a) Example with a misalignment percentage 0, and (b) example with 12% misaligned picture elements.

functions are shown in Figs. 2(d)-6(d) as pseudo-three-dimensional plots. As can be seen, some high-frequency fluctuations caused by noise and the fringe pattern itself remain in these reference images. This means that a lower cutoff frequency of the low-pass filters would be advisable in further studies. This, of course, can only be achieved by means of an increased computational cost if convolutional filter algorithms are used. Recursive digital filter techniques—possibly separable, with coefficients which are powers of 2—could circumvent this high computational burden.

A misalignment measure applied to the binary interferograms

The objective of the work described here is to produce a measurement value for a given binary fringe pattern that represents the deviation of this pattern from its corresponding "idealized" version. From Fig. 2 it can be seen that the fringe pattern of a flat surface region results in well-aligned fringe lines. In this paper it is assumed that the fringe lines of a flat surface have a vertical orientation, which can be achieved, e.g., by a proper calibration of the interferometer reference mirror. Defects on the surface cause some deformation of these lines (Figs. 3-6), i.e., some misalignment within these lines. It is the degree of this misalignment which is calculated by the measurement described in the following paragraphs.

Given is a binary two-dimensional pattern b(m,n) with $M \times N$ picture elements. This pattern is defined as an "ideally aligned pattern" if and only if all N pixels within an arbitrary

column m have the same values; i.e., all N pixels are black or all N pixels are white within column m, with $m = 1, \dots, M$. An example of such a pattern is shown in Fig. 8(a), in which the percentage of misaligned pixels is 0. In order to determine the percentage of misaligned pixels, it has to be determined whether each column m is to be considered a black or a white column. This decision is based on the predominant pixel value within the column; i.e., if column m has k_m white pixels and $N-k_m$ black pixels, it is considered to be a white column if $k_m > N/2$ and black otherwise [see Fig. 8(b)]. Subsequently, all white pixels in black columns and all black pixels in white columns are counted and the sum divided by $M \times N$, the total number of pixels. This ratio represents, according to the definitions above, the percentage of misaligned picture elements. For the fringe patterns shown in Figs. 2-6, this misalignment measure results in Interferogram 1: 5%, Interferogram 2: 8%, Interferogram 3: 15%, Interferogram 4: 16%, Interferogram 5: 42%.

As can be seen, these numbers reflect fairly well the degree of deformation of the fringe lines. However, a certain offset seems to be inherent in these percentages. It is rather obvious that this offset is mainly due to the noisy borders of the fringe lines. In order to avoid this influence, such noisy border columns have to be excluded from the misalignment measurement. To this end measurement masks have to be derived. This can be achieved in the following way.

Suppose the columns have been defined as black or white depending on the predominant pixel values and have been

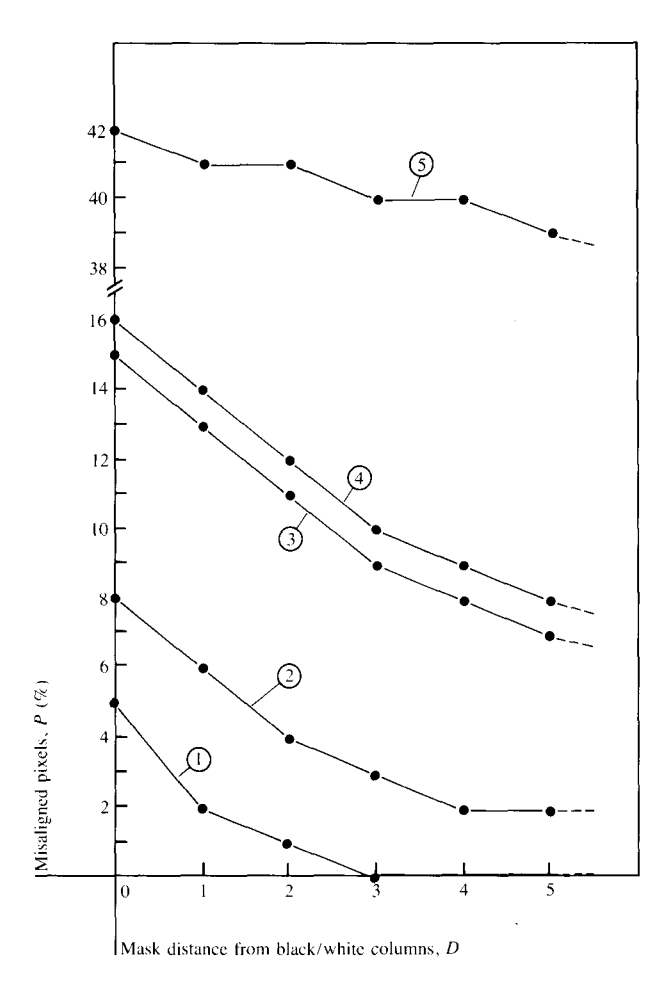


Figure 9 Misalignment measure results for the interference patterns (1)-(5) shown in Figs. 2-6 as a function of the distance parameter D.

denoted according to this condition by a sequence of B's and W's. A measurement mask is now defined which includes only those columns in the measurement which have at least a distance of D columns to a B-W-column adjacency. This is illustrated with the examples in Table 1, where \$ denotes whether the corresponding column is included in the measurement.

Using this scheme, the noise offset of the misalignment measure can be suppressed. The percentage of misaligned pixels as a function of the parameter D can be seen in Fig. 9. By taking the measurement only over the masked columns, a further advantage is obtained in decreasing the computational load for calculating the percentages. The number of columns involved in the measurement as a function of the mask distance D from adjacent B-W columns can be seen in Fig. 10.

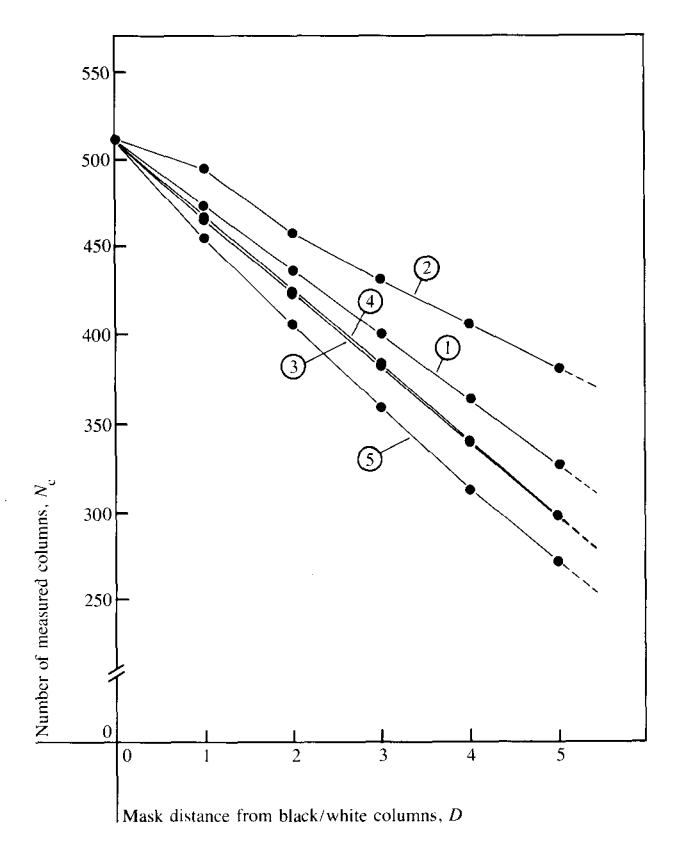


Figure 10 Number of measured columns versus distance parameter D for interferograms.

Conclusions

A hybrid optical-digital image processing method has been proposed for high-precision surface inspection. The technique uses an interferometer to image microscopic surface defects. In order to quantify the degree of various surface defects, the interferograms are scanned, digitized, and converted into a binary image by comparison with a spacially varying threshold reference image, which represents the inhomogeneity of the imaging system. A new misalignment measure for the binary patterns identifies the "straightness" of the fringe lines, and it has been shown that the resulting percentage of misaligned picture elements conforms fairly well with the degree of various surface defects. Our proposed measurement technique can be used in manufacturing inspection as a fast method to first determine whether or not a surface has any defects. Implementation of the misalignment algorithm can be done so that it operates at the TV scanning rate with special hardware. If a more detailed characterization of the defects is required, other more sophisticated analysis has to be performed, e.g., to identify the types of defects, such as asperities, holes, scratches, roughness, etc.

Table 1 Distances to B-W-column adjacency.

Column Type: W W W	w	w	w	В	В	В	В	В	В	В	В	w	В	w	w	w	w	w	w	w	В	В	В	В	В	В	В	w	В	w	w	
D = 0: \$ \$ \$ \$	\$	\$	\$	\$	\$	\$	\$	\$	\$	\$	\$	\$	\$	\$	\$	\$	\$	\$	\$	\$	\$	\$	\$	\$	\$	\$	\$	\$	\$	\$	\$	
D = 1: \$ \$ \$ \$	\$	\$			\$	\$	\$	\$	\$	\$				\$	\$	\$	\$	\$			\$	\$	\$	\$	\$						\$	
D = 2: \$ \$ \$ \$	\$					\$	\$	\$	\$						\$	\$	\$					\$	\$	\$								
etc.																																

References

- S. Tolansky, Multiple-Beam Interferometry of Surfaces and Films, Oxford University Press, London, 1948.
- S. Tolansky, Surface Microtopography, Interscience Publishers, London, 1960.
- M. Francon, Optical Interferometry, Academic Press, Inc., New York, 1966.
- E. Hohn, "Leitz Incident-Light Interference Illuminator for the Orthoplan/Metalloplan, A model which Uses the Wave Length of Light for Measurement," Leitz Scientific and Technical Info. VI, 8, 294 (1976).
- K. R. Castleman, *Digital Image Processing*, Prentice-Hall, Inc., Englewood Cliffs, NJ, 1979, pp. 303-313.

Received January 7, 1983; revised March 18, 1983

Samuel S. So IBM General Products Division, San Jose, California 95193. Dr. So is an advisory physicist in the Disk Technology Department of the Development laboratory, working on the surface finish characterization of future direct access storage devices. He joined IBM in 1965 at Endicott, New York, and worked on computer analyses of thermal diffusion, electron microanalysis, and holography. From 1968 to 1970, he was on educational leave and did his Ph.D. thesis in ellipsometry at the Materials Research Laboratory of Pennsylvania State University. In 1971, Dr. So joined the Advanced Technology Department of the Office Products Division in San Jose and worked on photoconductor and display characterizations. In 1974, he spent one year at the IBM UK Hursley Laboratory and worked on special ellipsometric analyses for multilayer thin films. In 1977, he joined the General Products Division in San Jose and worked on magnetic bubble memories until 1981. Dr. So received his B.S. from Duke University (1962), his M.S. from Florida State University (1964), and his Ph.D. from Pennsylvania

State University (1971), all in physics. He is a member of the American Physical Society, the Optical Society of America, and SPIE—The International Society for Optical Engineering. Since 1981, he has been conducting minicourses at the SPIE Symposia.

Friedrich M. Wahl IBM Research Division, Säumerstrasse 4, 8803 Rüschlikon, Switzerland. Dr. Wahl studied electrical engineering at the Technical University of Munich, where he received his Diplom and his Ph.D. in 1974 and 1980. In 1974 he started a digital image processing group at the Institute of Communication Engineering at the Technical University of Munich. He carried out many projects in the areas of image restoration, segmentation, and image analysis. From 1981 to 1982, Dr. Wahl worked on problems of document analysis and automated inspection by machine vision in the image processing project at the IBM Research laboratory in San Jose, California. Dr. Wahl joined IBM in 1983 at the Research laboratory in Rüschlikon, Switzerland. His recent research interests have been in the areas of image processing and image understanding, pattern recognition, image processing, hardware and algorithms, and systems for office automation. Dr. Wahl is a member of the Institute of Electrical and Electronics Engineers.

Kwan Y. Wong

IBM Research Division, 5600 Cottle Road, San Jose, California 95193. Dr. Wong received his B.E. (with honors) and his M.E. in electrical engineering from the University of New South Wales, Sydney, Australia, in 1960 and 1963. Since he received his Ph.D. from the University of California, Berkeley, in 1966, he has been working at the IBM Research laboratory in San Jose. He was the leader on projects in process control systems, air-jet guiding for flexible media, and image processing. Currently he is the manager of the image processing project in the Computer Science Department. His recent research activities are in the areas of image processing and pattern recognition systems for office automation, manufacturing automated visual inspection systems, special image processing hardware, and algorithms.